Naval Research Laboratory

Washington, DC 20375-5320

NRL/MR/7210--06-8932

Throughput Characterization of the NPOI Optical Train: Procedures and First Results

XIAOLEI ZHANG

Radio/Infrared Optical Sensors Branch
Remote Sensing Division

January 13, 2006

REPORT DOCUMENTATION PAGE

Form Approved
OMB No. 0704-0188

1. REPORT DATE *(DD-MM-YYYY)*	**2. REPORT TYPE**	**3. DATES COVERED** *(From - To)*
13-01-2006	Memorandum Report	Dec 04 - Oct 05

4. TITLE AND SUBTITLE

Throughput Characterization of the NPOI Optical Train: Procedures and First Results

5a. CONTRACT NUMBER

5b. GRANT NUMBER

5c. PROGRAM ELEMENT NUMBER
0601153N

6. AUTHOR(S)

Xiaolei Zhang

5d. PROJECT NUMBER
SP 034-6-41

5e. TASK NUMBER
T036-04

5f. WORK UNIT NUMBER
72-7187-06-5

7. PERFORMING ORGANIZATION NAME(S) AND ADDRESS(ES)

Naval Research Laboratory, Code 7218
4555 Overlook Avenue, SW
Washington, DC 20375-5320

8. PERFORMING ORGANIZATION REPORT NUMBER

NRL/MR/7210--06-8932

9. SPONSORING / MONITORING AGENCY NAME(S) AND ADDRESS(ES)

10. SPONSOR / MONITOR'S ACRONYM(S)

11. SPONSOR / MONITOR'S REPORT NUMBER(S)

12. DISTRIBUTION / AVAILABILITY STATEMENT

Approved for public release; distribution is unlimited.

13. SUPPLEMENTARY NOTES

14. ABSTRACT

An experimental procedure was developed for the systematic characterization of the throughput performance of the Navy prototype optical interferometer (NPOI). In this memorandum report, a detailed description of the measurement procedure and hardware, as well as the first results of the throughput measurement and analyses, are given. Recommendations for future tests and upgrades are made.

15. SUBJECT TERMS
Optical interferometry
Throughput measurement

16. SECURITY CLASSIFICATION OF:			**17. LIMITATION OF ABSTRACT**	**18. NUMBER OF PAGES**	**19a. NAME OF RESPONSIBLE PERSON**
a. REPORT	**b. ABSTRACT**	**c. THIS PAGE**			Xiaolei Zhang
Unclassified	Unclassified	Unclassified	UL	36	**19b. TELEPHONE NUMBER** *(include area code)* (202) 404-2389

Standard Form 298 (Rev. 8-98)
Prescribed by ANSI Std. Z39.18

CONTENTS

1 Background

Various earlier attempts at measuring the throughput of NPOI optical system using starlight photometry indicated that its value is in the range of 1-5%. Laser double-pass measurements of the front-end optical train up to the beam compressor, as well as the beam-combiner-table individual surface transmissions, suggested that the overall throughput contributed by these segments of the optics is around 50% (see the memo by R. Lucke 2004, which gave an order-of-magnitude summary of some of the past throughput measurements done by, e.g., Dave Mozurkewich and Jim Benson).

The apparent transmission from the input of the lenslet array to the APD is on the order of 1 (J. Benson, private communication), a result clearly indicating that the APD afterpulsing and other factors contributed to inflating the apparent pulse counts, since we know for certain that there exist various contributors to throughput loss in this segment of the propagation path, including the lenslet array coupling loss, the fiber coupling and transmission loss, APD quantum efficiency and photon detection probability, etc., so the overall effect of these losses must have added up to cancel the effect of afterpulsing and other gains. The existence of the artificial gain mechanisms clearly complicates any attempt at estimating the system throughput by using the stellar photometry on the APD readout alone.

Recently, Henrique Schmitt did a thorough analysis of the photometry data taken around 2004-01-30. The new analysis once again gives the apparent throughput for all beam lines in the range of 1-3%, agree with prior estimates.

Note that these earlier estimates of the overall system throughput (i.e., the 1-3% numbers) did not take into account the possible effect of APD afterpulsing, which at the moment is an unknown. If the APD afterpulsing rate is significant, the actual throughput value can be significantly less than the above estimates.

The throughput measurements conducted so far either suffered from the uncertainties introduced by the APD characteristics, or else are not conducted in a systematic manner covering the entire optical train and spectral bandpass, and breaking the measurement up into segments, thus allowing us to pinpoint the major contributors of the throughput loss. It is thus desirable to design a new set of experiments for a thorough and quantitative assessment of the spectral throughput response of the various NPOI optical-train

Manuscript approved November 7, 2005.

segments, with results that are independent of the gain mechanisms of the detectors. The tests described in this memo would satisfy these requirements.

2 Test Procedures

2.1 Overview of Proposed Throughput Tests

There are two sets of planned tests. The first set of tests makes use of the artificial whitelight and laser sources on the beam combiner table, and characterizes the spectral throughput responses of the different segments of the NPOI optics by making differential total power measurements, using both a CCD with a set of interference filters mounted on a filter wheel, and a laser power meter. Most of these tests will be conducted in auto-collimated, double-pass configurations of the optical train.

The second set of tests makes use of the celestrial stellar sources of known spectral energy distribution to perform single-pass radiometry measurements, again using a CCD fitted with a set of spectral filters. This complementary set of tests will help tie together the stellar flux scales to the observed photometric response of the NPOI, passing through the different segments of the NPOI optical train.

2.2 Test Setup

In order to minimize the potential impact on the existing optics on the NPOI optical train, especially those on the beam combiner table, most of the test optics and computer equipment will be located away from the existing NPOI optical train. The test optics will be set up on a so-called ScienceDesk by MellesGriot (Figure 1), which is a reduced-sized version of the conventional optics table with passive vibration damping, and has a separable tie-bar frame with castors which can be lowered down during the transport of the whole unit. The ScienceDesk we have procured has a 2.5'x3' breadboard which will allow it to be fit into the various locations in the inner room, including near the beam combiner table, but has enough area to accommodate all the planned optics setup.

The beams on the beam combiner table at different locations will be

Figure 1: ScienceDesk from MellesGriot

brought out of the table by a Newport beam-steering periscope assembly (Figure 2), which has relatively small footprint and can be inserted into the beam path to intercept and redirect the beam to the ScienceDesk. The periscope also helps to raise the beam height so it can get out of the insulation on the sides of the beam combiner table. Since at each location there will in general be 9 measurements made (laser power, laser reference power, 450nm, 500nm, 600nm, 700nm, 800nm bandpass whitelight, wideband whitelight, and whitelight reference), the overhead of having to clamp the periscope down and fine-adjust its azimuth and elevation to feed it into the measurement optics setup on the ScienceDesk is justified, especially this approach results in the smallest footprint on the beam combiner table and the least chance of damage to the existing optics.

On the ScienceDesk (c.f. Figure 3), a Newport broadband beam splitter will split the laser or whitelight beam into two paths. One path feeds the laser powermeter head through a focusing Fabry lens pair. The other path goes through a couple filterwheels (with ND and BP filters mounted) to a focusing lens which feeds the whitelight signal into the CCD camera. Note that during either the laser or the whitelight power measurements the other source needs to be blocked off, yet with this beam splitting arrangement we do

Figure 2: Newport Periscope Beamsteerer

not have to rearrange the test optics, and the split-off laser signal also helps the alignment of the CCD. Also note that even though the Fabry lens pair makes the image spot on the laser powermeter head stationary with respect to the angular directional changes of the incoming beam, the image spot still shifts if the beam lateral position is not the same each time. This, plus the fact that the powerhead sensitivity is not uniform across the area, leads to uncertainties in the readout results. We will thus use the laser powerhead readout only as a reference and a sanity check. Even when we do record laser power levels, we will use the one given by the CCD. The periscope on the ScienceDesk helps to lower the beam height and redirect the beam to the two feed mirrors which together have enough degrees-of-freedom for beam directing so that the rest of the optics starting from the beam splitter will not need to be realigned each time we change to a new measurement location.

Apart from the parts mentioned above, a stand-alone PC with monitor will be used in the data acquisition. The computer has a PCI slot which will accommodate the framegrabber card (NI PCI-1428) which is interfaced to the CCD camera. The data acquisition for the CCD will use custom software written based on National Instruments' LabWindows/CVI package (similar to Labview in the user interface but uses C language for the programmer's

interface). More detailed instructions on using the data acquisition software is given in Appendix D.

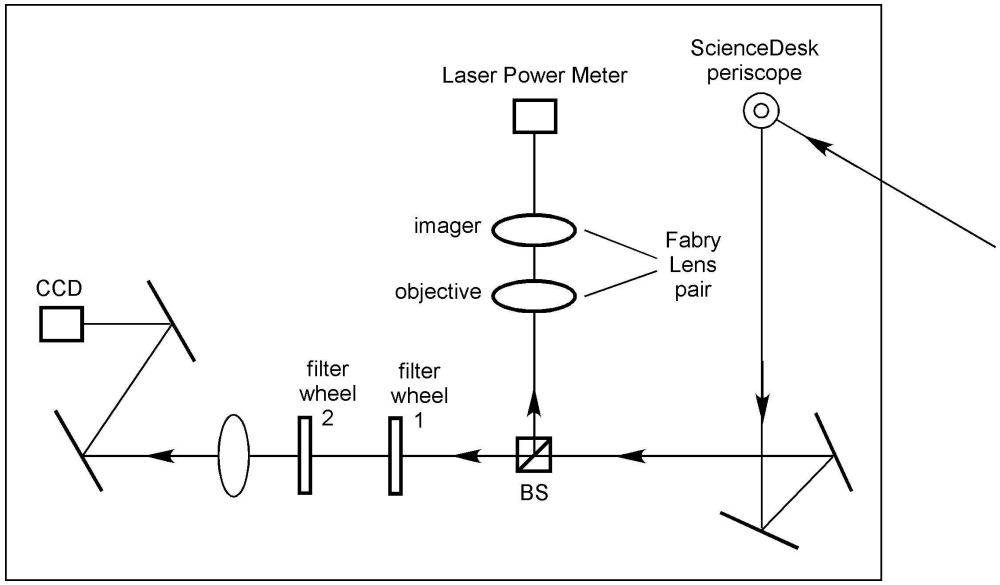

Figure 3: Schematics of the Optics on the ScienceDesk

2.3 Test Approaches Using Laser and Artificial Whitelight Sources

The first set of tests will make use of the output of the artificial whitelight and laser sources on the beam combiner table, in both double-pass (see Steps 1-3, and Step 5 below) and single-pass (Step 4) configurations. Differential power readouts at the different locations will allow us to estimate the throughput loss of the corresponding optical segments.

Before proceeding to describe the test procedures, we indicate in Figure 5 below the locations for setting up the laser beam polarizer and half-wave plate, laser reference power readout, and the ND filter for NAT path power attenuation (this ND filter was commonly implemented at the immediate output of the whitelight source. But since we wanted to maintain the maximum useable whitelight power to improve S/N during double-pass measurements, we will temporarily put the ND filter in the NAT path directly to assist its

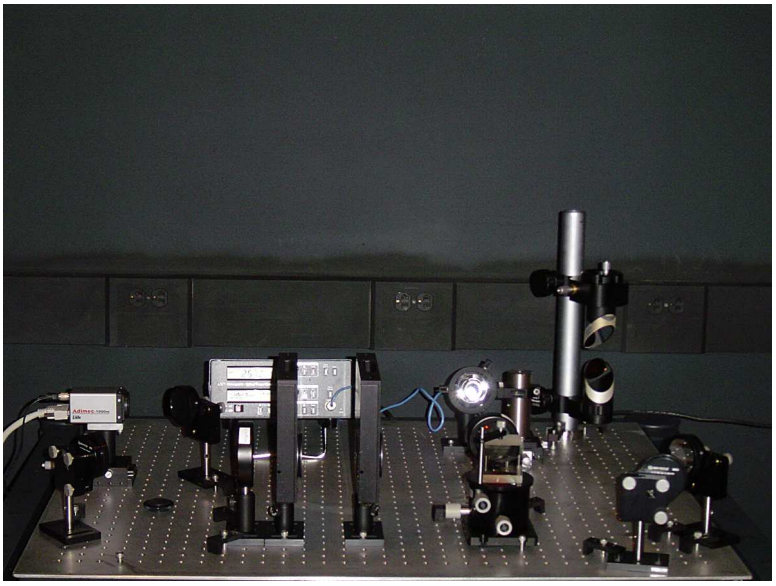

Figure 4: Completed Optics Assembly on the ScienceDesk

tracking).

The polarizer and half-wave plate will only be used if there is time available at the end of other proposed tests, in order to characterize the polarization throughput response of the system. Not doing this set of test will not impact the integrity of the rest of the proposed tests. Currently with the mounts we envisioned both components should fit in the indicated place without the removal of existing beam combiner optics.

The double-pass differential power measurements will be done in the autocollimation mode. We will do the autocollimation in three locations: at the output of the beam combiner table; on the switchyard table after the beams have gone through the FDLs; and at the SID mirrors. In the following we describe the different segments of the test procedures in "Steps". These steps are not necessarily the order that actual experiments will be carried out. For a detailed description of the proposed daily schedules of tests please refer to Appendix A .

Step 1: (refer to Figure 6)

In this step we set up the the autocollimating mirrors at the output of

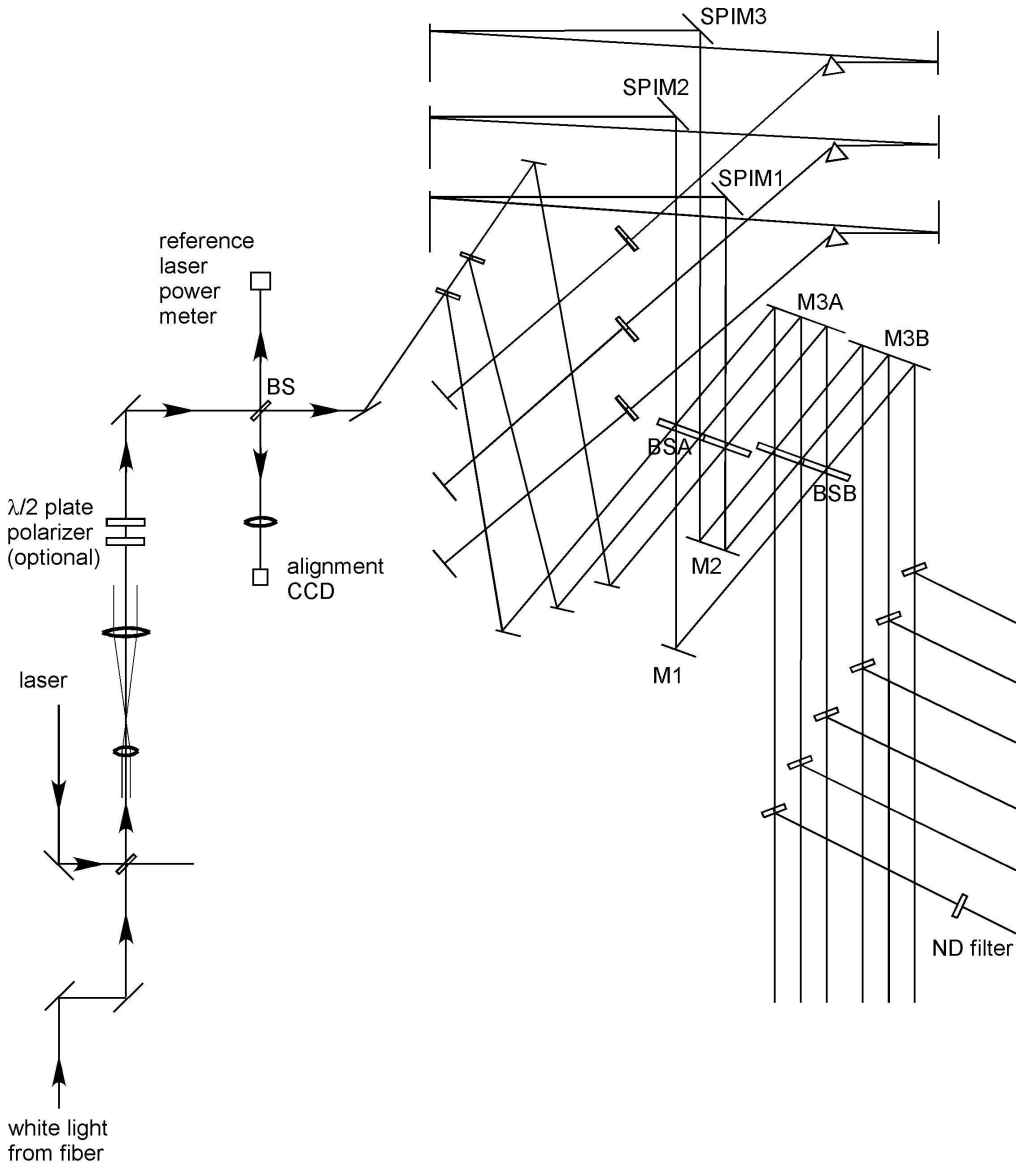

Figure 5: Auxiliary and Reference Setup On the Beam Combiner Table

the beam combiner as shown in Figure 6. The sampling location 1,2,3 are the first ones where the double-pass return beam can be sampled without blocking the outgoing beams. From here on the beams will experience only single pass, and the measurements locations indicated on Figure 6 which will allow us to characterize the throughout performance of the paraboloids, prisms, pinholes and achromat lenses.

At the converging or diverging locations of the beams a lens of varying focal length (either positive or negative) will be used to recollimate the beam.

We also plan to record at marked location 10, with and without the pinhole in place, in order to better assess the pinhole throughput, compare and confirm with the corresponding measurement using the lens to recollimate the beam.

Step 2: (refer to Figure 7)

The loss due to the FDL propagation paths can be assessed by comparing the return signals measured on the beam combiner table, at locations as marked in Figure 7 for the respective beam lines, with the autocollimation mirror located first outside the beam combiner table, and subsequently in front of the FDL. While autocollimating at the FDL, the delayline lengths can be varied to check out the effect of propagation length on throughput (thus the effect of scattering loss due to small-scale irregularities of the mirror surfaces), as well as the effect of residual misalignment of the optics on throughput.

Step 3: (refer to Figure 8)

Subsequent autocollimation of the SID mirrors, and the comparison with the result of autocollimation before the FDLs, allow the assessment of the propagation loss of the front-end optics from the FDL to the SID mirror. Once again, the measurement location is as marked in the Figure, and the measurement will be done for every beam line.

Step 4: (refer to Figure 9)

In order to characterize the performance of the science beam splitters BSA and BSB (refer also to Figure 5), and some of the relay mirrors, the outgoing-beam power (in single-pass) will be measured at some of the accessible locations as indicated in Figure 9. Unfortunately, most of the desired locations for this step are not accessible by the periscope. But fortunately,

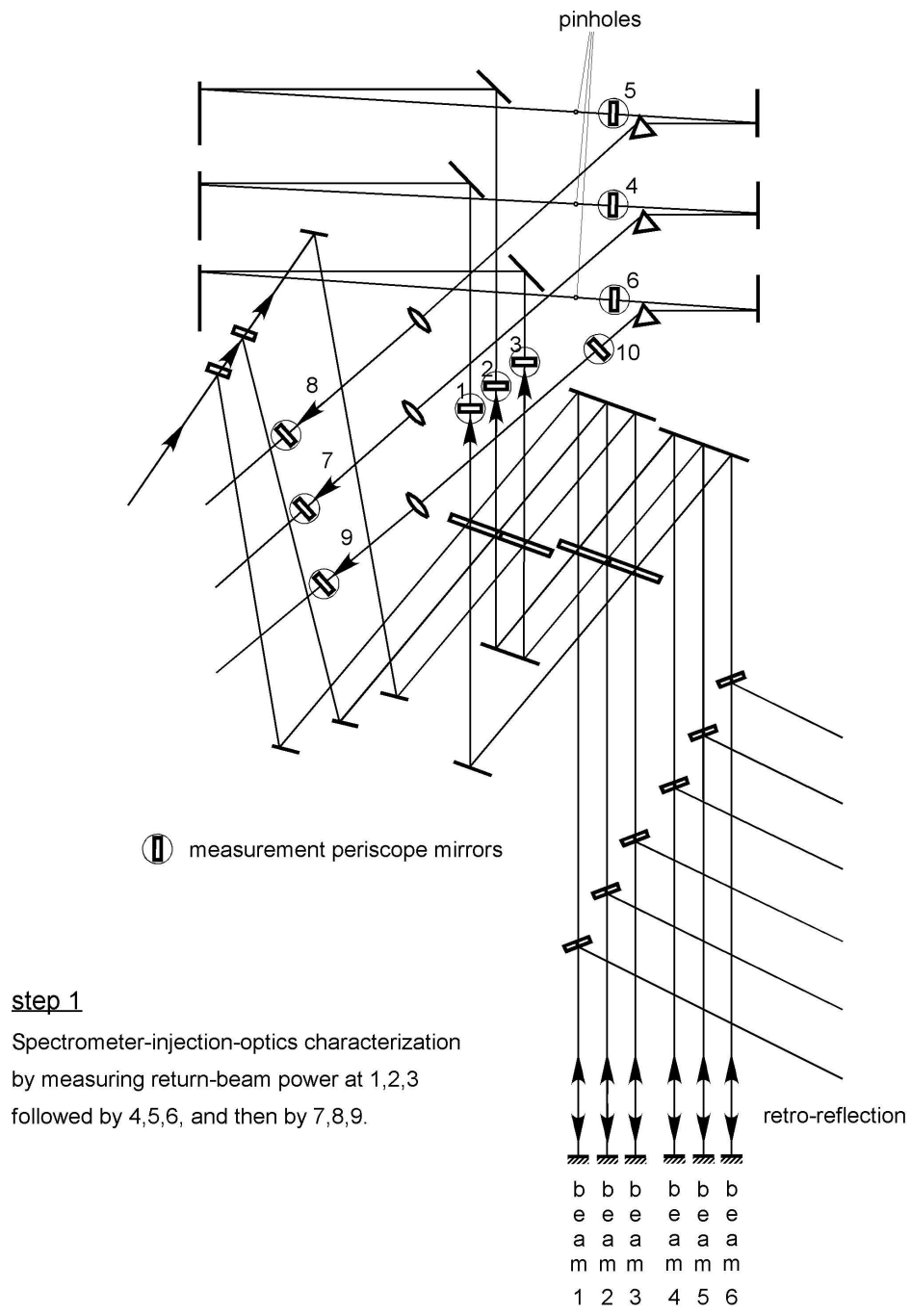

Figure 6: Test Configuration for Characterizing the Throughput of the Spectrometer Injections Optics

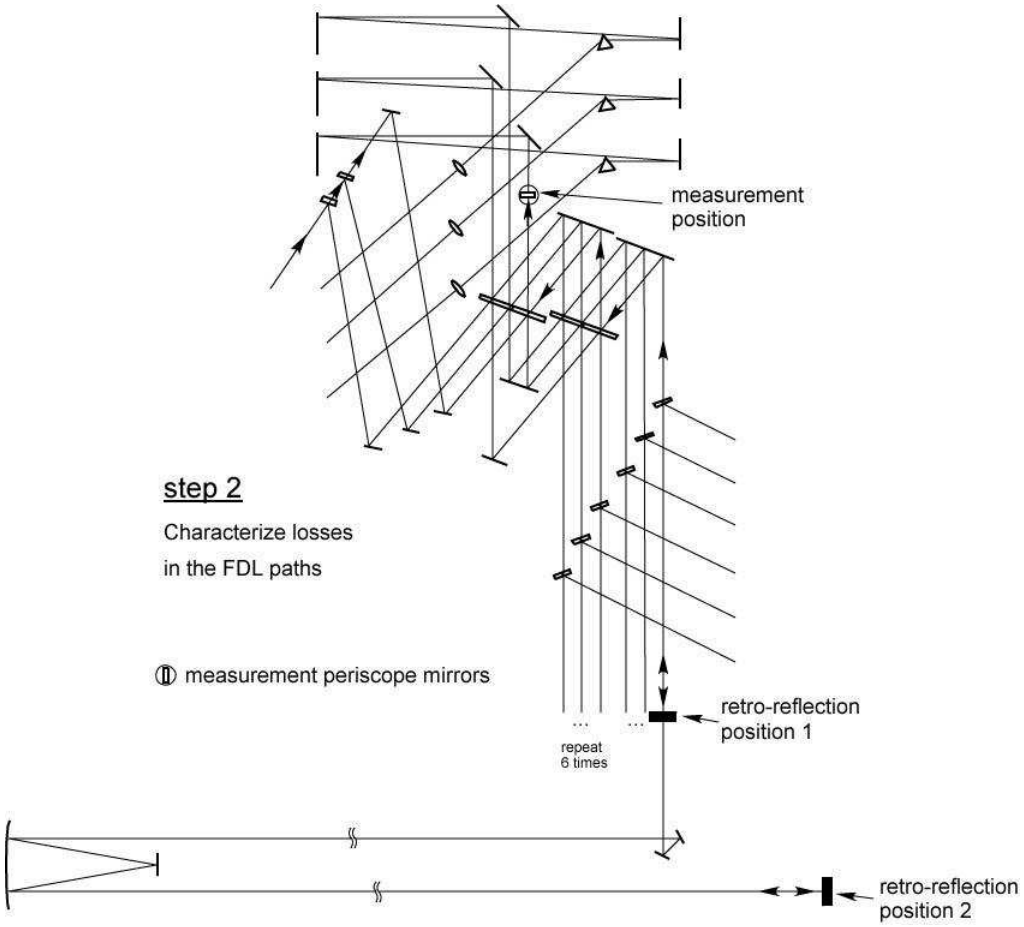

Figure 7: Test Configuration for Characterizing the Throughput of the Fast Delay Line (FDL) Paths

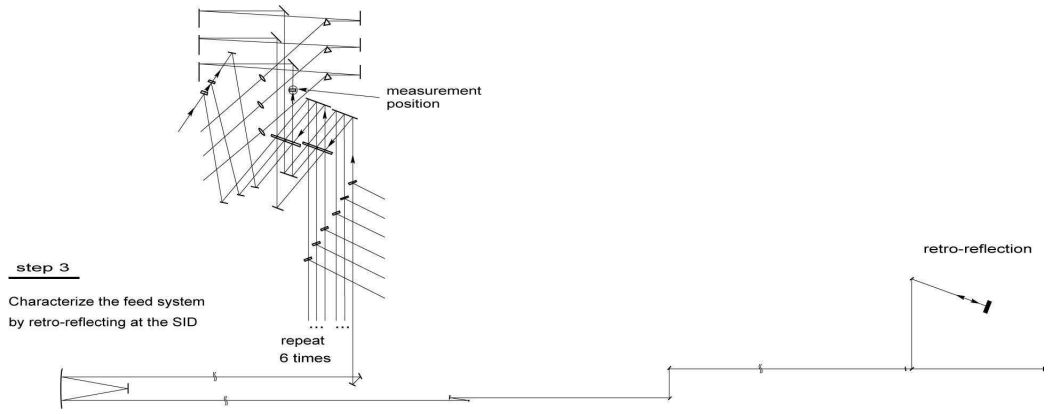

Figure 8: Test Configuration for Characterizing the Throughput of the Feed System

this leg of the transmission path is not our biggest suspect of the throughput loss, and we will get an overall transmission between 1 and 2 as indicated in Figure 9

Step 5: (refer to Figure 10)

In order to measure the spectral throughput response of the lenslet array and fiber path, we need to disconnect the fiber connector leading to the APD so as to measure the output power directly from the fiber. A custom multimode fiber from Fiberguide Industries has been ordered, of 50 feet length, enough for it to be connected to the fiber connector in the electronic room, and thread it through the mousehole on the wall and into the inner room so the light can be channeled to the ScienceDesk optics. This fiber is made by the same company which made our original fibers, but the new fiber is of slightly larger core diameter so all the light can be collected and channeled into the measurement setup.

A custom mount structure is made to hole the fiber holder which is mounted rigidly with respect to the lens holder used for collimating the output beam from the fiber, so it can be directed to the ScienceDesk input optics (by passing however the ScienceDesk periscope).

The proposed number of whitelight fiber throughput measurements, as suggested by the design review committee, will be of four fiber channels on

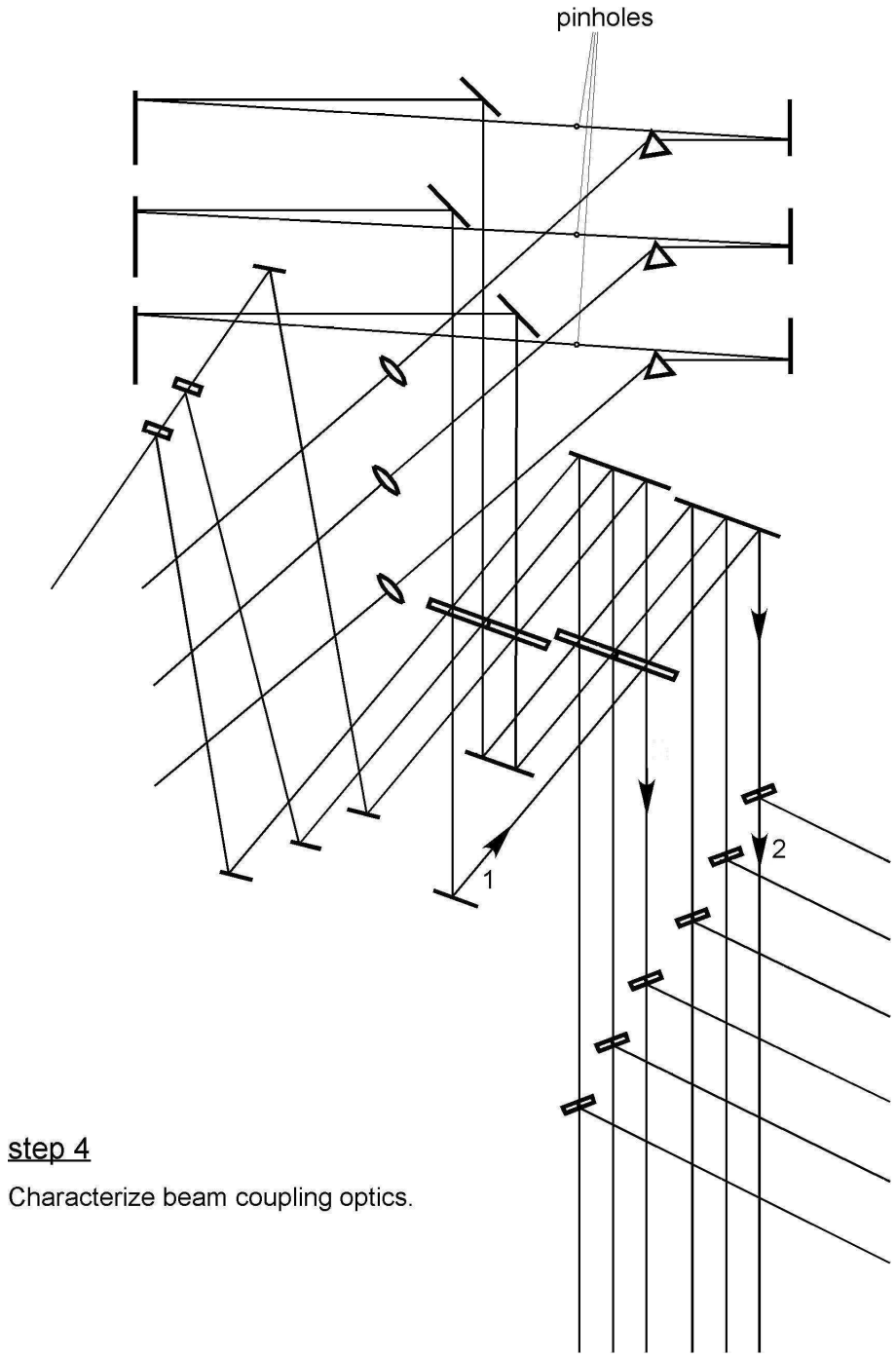

Figure 9: Test Configuration for Characterizing the Throughput of the Beam Combining Optics

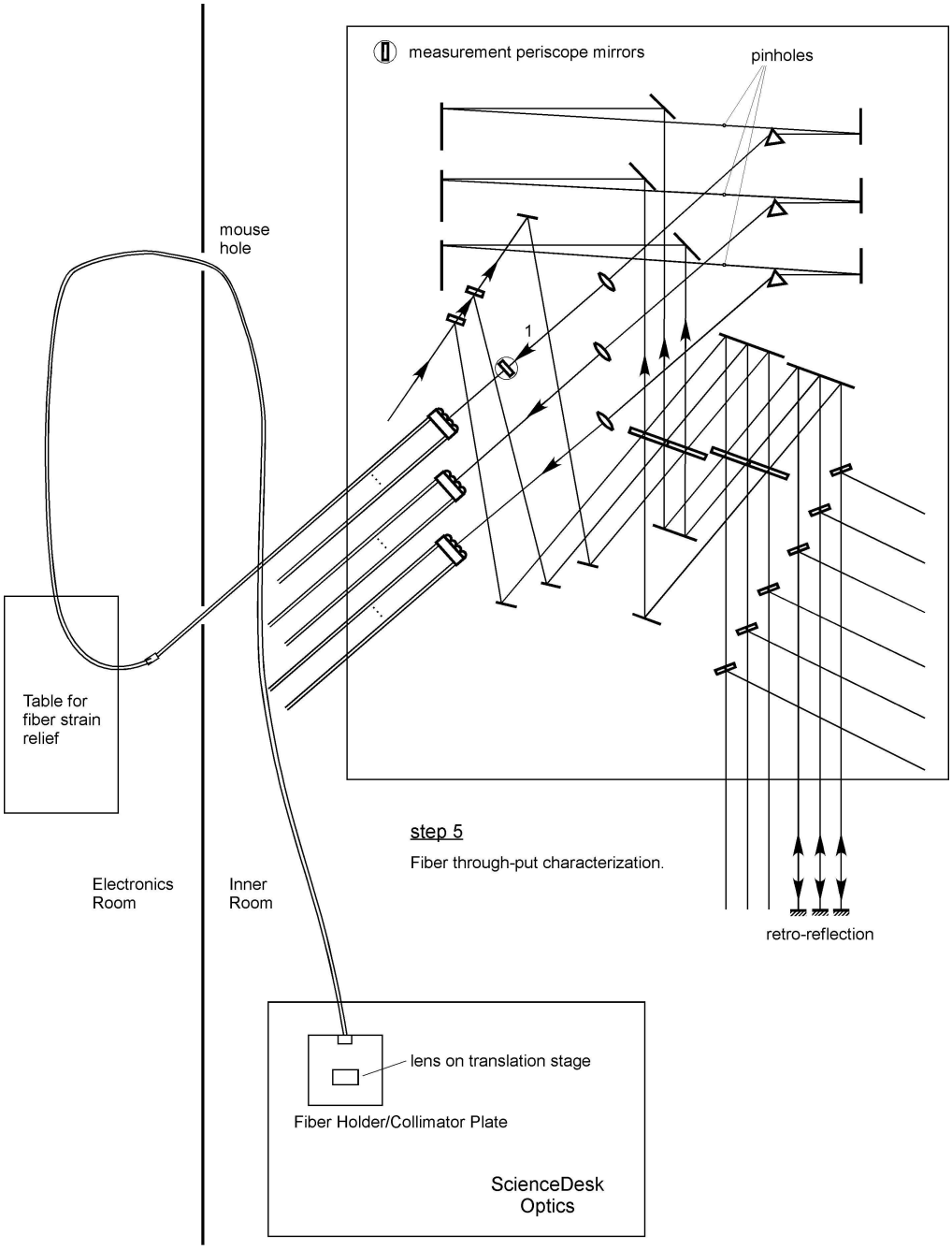

Figure 10: Test Configuration for Characterizing the Throughput of the Fiber Injection and Propagation Paths

one spectrometer. One each at the red and blue end, and one each for channel 10 and 20. Currently we propose to use spectrometer 3, since that was one which have APD connected to all its channels.

We also propose to scan laser input beam onto the lenslet array across all spectrometer channels (by manually translating the lenslet array), and to record the readout by embedded system in order to compare the relative throughput of the channels in the spectrometer at the HeNe frequency. This step does not require the disconnection of any fibers, but will not give the spectral dependence of the fiber transmission, only the relative transmission of all channels at the laser frequency.

2.4 Test Approach Using Astronomical Sources

The second set of whitelight throughput tests will make use of bright stars of known spectral energy distribution to enable absolute radiometry in a series of 5 passbands across the visible spectrum, using different bandpass filters mounted on a filter wheel, at the various locations along the beam lines after the beam compressors (so we only need to deal with the 1.4 inch beam size). It will be done in conjunction with the Risley prism test.

In order to facilitate the star acquisition onto the CCD camera (of model Adimec-1000m, which is a megapixel, 50 frames/sec, high QE CCD using a Kodak chip, which we have already purchased), and also in order to allow simultaneous angle tracking and backend spectrometer/APD recording while conducting the whitelight throughput test, we have procured a custom plate beam splitter which has transmission beam deviation tolerance of +-2", from a company called Precision Glass and Optics in CA, which can be used to intercept the beams along the beam lines at various locations. The beam splitter will initially be used with the alignment laser in the normal alignment procedure to channel the laser beam onto the CCD detector to help with its alignment, and which will later be left in place to split off 50% of the starlight to feed the rest of the whitelight test optics on the ScienceDesk.

The first tests using the astronomical sources (see Figure 11) will be done near the so-called "IR switchyard table", which is located on the west side of the beam compressor table, and which is currently unpopulated so we plan to use it for the eventual permanent installation of the six sets of Risley prisms. The beam splitter used for picking the light off the stellar beam will be mounted on a tilt/rotation stage which in turn resides on a labjack.

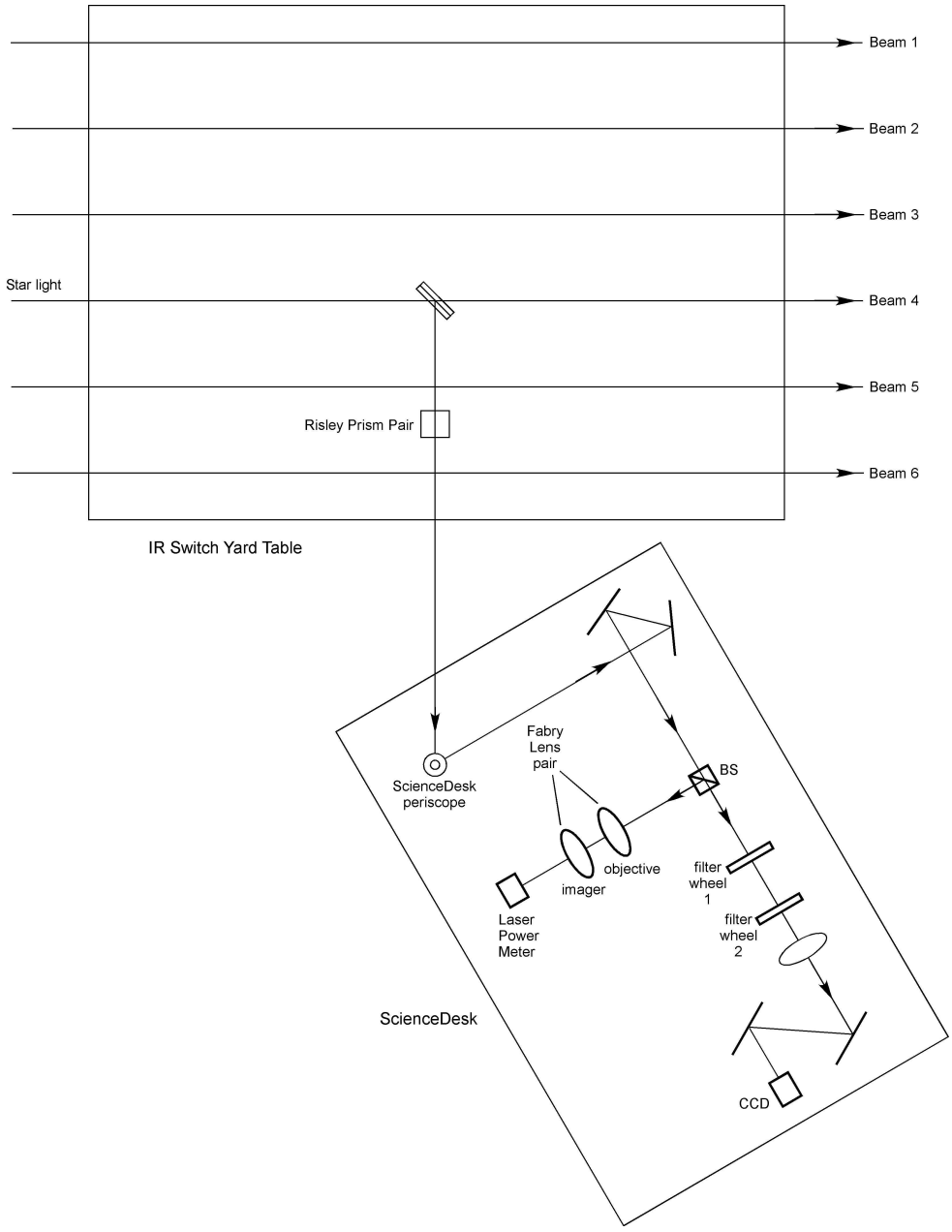

Figure 11: Test Configuration Near the IR Switchyard Table for Absolute Photometry and Risley Prism Tests

The Risley prism itself will be supported by a larger labjack. Both the beam splitter and the Risley prism assemblies will reside on the IR switchyard table during the planned tests. The coupling of the beam onto the ScienceDesk may require the removal of the periscope and replace it with a single mirror in a mount.

3 Results of the First Phase of Measurements

3.1 Overview of the Tests

The throughput measurements of the NPOI optical train conducted during the week of August 8, 2005 is the result of one year of preparation effort as well as several design review iterations. Due to time constraints and also the low flux of the existing whitelight source on the beam combiner table, only laser throughput measurements have been conducted during this first week of throughput test. Whitelight, spectral throughput measurements using narrow-band filters are planned for the near future. So is the single-pass, absolute photometry and throughput measurement using stellar sources.

The week of August 8, being in the middle of the Monsoon season, did not allow the opening of the two imaging siderostats (SIDs) at night to do the feed system throughput measurement for these stations. We have only obtained the throughput measurements of the four astrometric feed systems since the SID mirrors for these four stations are located in closed domes.

Also partly due to the time constraint, and partly due to safety precautions, only one spectrometer path (that of spectrometer 3) and selected fiber/APD channels have been measured for throughput.

3.2 Characterizing the Fast Delay Lines (FDLs)

The throughput of the Fast Delay Line (FDL) segment of the optical path was obtained through the differential flux measurements in double-pass retroreflection configurations (Step 2 in section 2), with the first retroreflection point at the input of the beam combiner table/output of the switchyead, and the second retroreflection point at the input of the delay line. We have performed this measurement for all six NPOI beams, and each differential measurement

was performed once for delay line cart parked in front (shortest delay), and once for delay line cart parked all the way back (longest delay). The double-pass difference in pathlength between the two parking positions is about 35 meters.

When calculating the throughput values for each pair of "before" and "after" measurements, we have compared the results given by the laser powermeter differential measurements, and the CCD differential measurements. These are found to track each other fairly well – the throughput given by these two instruments are usually within a couple percent if a short time average is made – for this particular set of measurements where both the "before" and the "after" beams are the 1.4 inch collimated beam. This agreement is impressive especially since the CCD is measuring flux at the image plane after the collimated beam is focusing by a lens, whereasthe laser powermeter is effectively measuring the flux at the aperture/pupil plane since a Fabry lens pair has been used to reimage the pupil. The agreement between the two shows that little flux in the sidelobes is lost due to the finite site of the integration box.

Here is a summary of the throughput measurement results for the six delayline paths, and two parking positions for each path, obtained through an average of the laser and CCD results. Note that the numbers below have been converted to the equivelent single-pass throughput values by taking the square-root of the original double-pass values as given by the raw data (though in actuality the the single-pass throughput may or may not be equal to the square-root of the double-pass throughput, especially in the presence of path-length-dependent throughput loss, which seemed to be the case for us):

Delayline 1: Front: 0.83 Back: 0.76
Delayline 2: Front: 0.82 Back: 0.73
Delayline 3: Front: 0.85 Back: 0.82
Delayline 4: Front: 0.86 Back: 0.84
Delayline 5: Front: 0.80 Back: 0.73
Delayline 6: Front: 0.86 Back: 0.80

The dependence of the measured throughput on the pathlength difference between the mirrors, as indicated by the different measured throughput values when the delayline cart is parked at the front or at the back, indicates that mirror reflectance loss is not the only contributor to the throughput loss, other factors such as scattering (due to small-scale roughness of the surface) and diffraction (due to wavefront curvature) may also have played a role.

Figure 12 plots the measured double-pass throughput results which indicate a possible correlation of the ratios of the delayline throughputs measured when the cart was parked at the front and at the back, versus the absolute throughput levels as represented by the throughput measured when the delayline was parked at the front. The data clustering in fact were better than indicated in the figure, as the range of display has been zoomed-in to show the difference. Possible causes of this dependence include the small-scale surface roughness of the mirrors, and the roughness of the vacuum windows. In effect the correlation shows that the surface roughness at the earlier part of a propagation path continues to exert an influence for the throughput degredation towards further propagation path.

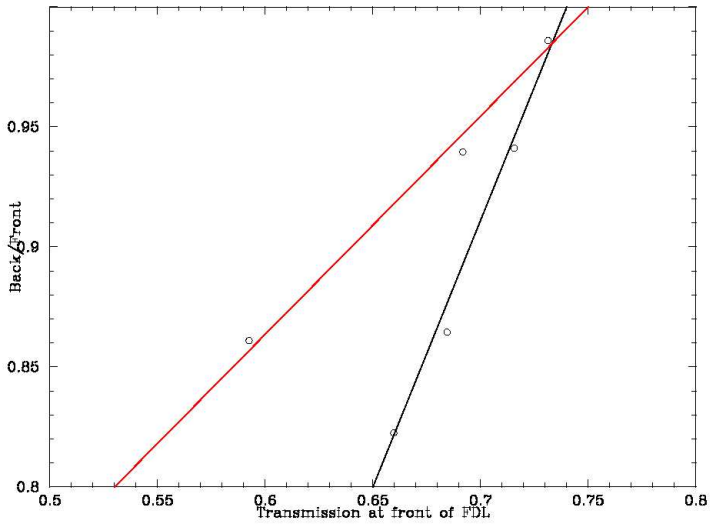

Figure 12: (Produced by D. Mozurkewich). Possible correlation of the ratio of throughputs of the FDL path when the cart is parked at the front and at the back of the FDL, and the throughput when the cart is at the front of the FDL. Note that in this plot the double-pass throughput values are used. The two lines drawn over the measured data points indicate two possible ways to fit the data.

3.3 Characterizing the Feed System

The feed system includes all the frontend optics prior to the FDL, i.e., the beam compressor optics, the periscope mirrors, the SID and NAT mirrors, and the vacuum pipe windows. The details of the measurement configuration is described as Step 3 in section 2. The two retroreflection positions for the differential measurement are, first, off the SID mirrors themselves, and second, off the autocollimation mirrors at the input of the FDLs. Due to the height of the measurement periscope on the beam combiner table, the Celotex cover on the beam combiner table cannot be closed during the throughput measurements, and the background light in the room prevented NAT loop from locking. Manual fine-centroiding of the image had to be done each time just prior to each measurement readout. The short-time stability of the system is good enough for the image to remain in the integration box during the measurement period every time.

Due to the same-sized collimated return beam measured at the backend, we had once again achieved high measurement accuracy, with the throughputs measured by the laser power meter and the CCD usually agree within a few percent of each other, and the repeatability for measurements done at different times were excellent.

The throughputs of the four astrometric feed systems are measured as follows (once again, we have converted the double-pass measurements to equivalent single-pass numbers by taking the square-root of the measured throughput. Averages have been taken of the respective laser- and CCD-measured throughputs):

Astrometric Center, on beam 2: 0.75
Astrometric East, on beam 3: 0.72
Astrometric West, on beam 4: 0.76
Astrometric North, on beam 6: 0.5

Here we can see that compared to the other three beamlines Astrometric North on beam 6 has abnormally low throughput. We have done visual inspections of the laser spot on the Astro North SID (seemed normal), repeated this measurement several times (with essentially the same result each time), and as of now we could not find the apparent cause of this anomaly.

The feed system propagation path is much longer than the FDL propagation path, yet the propagation loss for most of the beam lines is comparable for the two cases. This perhaps has something to do with the oversized optics

used for this segment of the optical path.

In Figure 13, another possible correlation of the throughput of the feedsystem with the differential throughput in the FDL path is indicated. If the correlation does correspond to a physical cause, it apparently continues the trend indicated in the FDL data that the roughness in the earlier part of the optics (i.e. FDL optics) continues to impact an influence towards later part of the optics (in this case the feed path). The correlation however is weak, as the data for the main part is quite flat apart from the one outlier. Additional data points from the two imaging stations will help settle the issue.

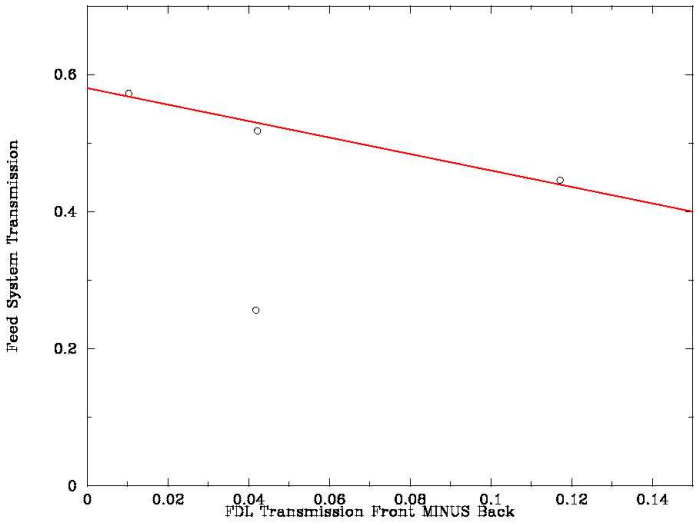

Figure 13: (Produced by D. Mozurkewich). Possible correlation of the feed system throughput with the differential throughputs of the FDL path when the cart is parked at the front and at the back of the FDL. Throughputs plotted are double-pass values.

3.4 Characterizing the Spectrometer Injection Optics on the Beam Combiner Table

The spectrometer injection optics contains optical elements such as the achromat, the two paraboloids surrounding the pinhole, the pinhole itself, the

dispersing prism, and one fold mirror. The detailed configuration for this segment of the test is described as Step 1 in section 2. Note that we have combined the two-stage measurement described in that document into a single-stage overall throughput measurement during the actual test, due mainly to time constraints.

The throughput in this leg of the path is 0.46 for spectrometer 3. This number was obtained as follows. The throughputs measured by the CCD at two different focus settings (and the accompanying integration time and ND filter settings) give an average throughput of 0.38. The laser powermeter gives a throughput of 0.54. Taking the average of the two values we arrive at 0.46.

This measurement is more uncertain than the FDL and feed system throughput measurements described before due to the fact that here beams of different sizes and collimating status are involved – one is the 1.4 inch collimated beam at the entrace of the beam combiner, and another is a converging beam at the input of the lenslet, being recollimated by a negative lens, forming a beam of roughly 0.5 cm diameter before being sent out to the ScienceDesk. Different-sized beams makes the laser power meter responses not being identical for the two differential measurements (since the different active regions in the laser power meter head has different sensitivity) – in fact we have to move the laser powerhead location and by-pass the Fabry lens pair for this set of measurements in order to better match the "before" and "after" beam sizes, but doing this we lost the angular insensitivity which was enabled by the Fabry lens pair . The CCD measurements, on the other hand, is made uncertain by the uncertainty in the nominal values of the ND filters inserted. So we have performed an average of the laser and CCD results to obtain the final value.

It is to be noted that the throughput in this leg will depend strongly on the alignment of the pinhole, and on the focusing of the system (as well as on seeing conditions in the case of stellar measurement). So this throughput number is expected to be variable and is more strongly alignment-dependent than the throughput values in other segments of the optical path.

3.5 Characterizing the Lenslet Array Injection and Fiber Throughput

The lenslet array injection and the first leg of fiber propagation path was originally suspected as a possible major contributor of the throughput loss, but as it turned out, the measured transmission is quite reasonable. The configuration for this test is described as Step 5 in section 2. In what follows we quote only the measurement results from the CCD, since the laser power meter once again does not have the same sensitivity for the "before" and "after" cases since the beams in the two cases were of significantly different sizes after collimation and reimaging. For the CCD measurements, on the other hand, we were able to defous the image on the camera for the lenslet array injection case so that it covers roughly the same area on the CCD as for the fiber-end image, and have similar surface brightness as well, so no additional ND filter needed to be inserted, and the integration time used for the two cases could also be set the same.

We have corrected about 3% of transmission loss for the 50 ft test fiber (which has a core diameter of 400 μm compared to our existing fiber's core diameter of 333 μm, thus can receive most of the photons being piped over), based on the manufacturer's specification sheet. A direct measurement of the fiber loss was not successful since the segments of fibers we attach onto the end of the 50 ft, 400 μm diameter fiber are also of 400 μ diameter, and the insersion loss in this case dominated any propagation loss.

The transmission at the HeNe laser frequency for the four fiber channels on spectrometer 3 are found to be:

Channel 1 of spectrometer 3: 0.65
Channel 10 of spectrometer 3: 0.83
Channel 20 of spectrometer 3: 0.78
Channel 32 of spectrometer 3: 0.81

The enslet array on spectrometer 3 was translated during this measurement so that the laser light can pass through each channel being characterized.

3.6 Loss Due to Beam Splitters

The science beam splitters on the beam combiner table had been characterized previously and found to be close to manufacturer's specs. We will thus use these specs for the beam splitter transmission and reflection, since both the accessibility of these locations needed for the beam splitter characterization, and the time constraints, prevented us from carrying out this measurement during the week of August 8. The locations for the intended measurements are described as Step 4 in section 2.

At the HeNe frequency, the transmission and reflection of the two sets of science beam splitters are 0.52 and 0.48, respectively.

The NAT coupling beam splitter is expected to induce a throughput transmission on the main path on the order of 0.8.

3.7 The Issue of APD Afterpulsing

The determination of the APD afterpulsing rate is important both for obtaining a reliable throughput estimate using the embedded system readout in the stellar photometry approach, and for assessing the APD performance itself.

We perform this measurement by estimating the input photon flux at the input of the last fiber segment leading to the APD detector, and comparing this flux with the value of the pulse rate given by the APD as read out by the embedded system (FringeCon, in this case). The measurement turned out to be complicated by the uncertainty of the precise values of the ND filters used in order not to saturate the APDs. So, we would need to treat the results in this section as tentative, pending on further calibrations of the ND filters and the repeated measurements of the input photon flux.

Here, we first report one example of such an estimate, for channel 32 of spectrometer 3, since for this channel we had measured the pulse rates using two different sets of ND filters (one case with two NDF4s, or a total transmission of 10^{-8}, another with one NDF4 and one NDF2.5, with a total transmission of 3.1×10^{-6}), and can cross-compare the results and get an estimate of the magnitude of uncertainties. After scaling of the results to obtain the equivalent zero-loss pulse rate measurements, these two settings gave $1.185 \times 10^{1}0$ pulses per 4 ms, and 4.58×10^{9} pulses per 4 ms, respectively.

These correspond to 3×10^{12} pulses per second, and 1.17×10^{12} pulses per second, respectively. Note that in obtaining these count rate we have corrected the wavelength scaling factor (1/0.633) which coverts the FringeCon reported count rate to the actual input count rate to take into account of the "measurement window" effect of the FDL strokes (even though the FDLs are not explicitly used for this measurement).

From the derivations in the Appendix, we know on the other hand that the conversion factor between the integrated count rate measured by the CCD and the photon flux is $\#\ of\ photons/sec = 286 \times (\#\ of\ integrated\ counts/sec)$ Therefore, since for channel 32 we measured the integrated CCD counts to be 6.05×10^6 per 2 milliseconds, this gives the estimates input photon flux as $8.65 \times 10^1 1$ per second. This number, however, is the measured photon flux at the entrance of the CCD, and not the photon flux at the entrance of the APD. For the APD flux we need to calibrate out the loss due to the transmission in the ScienceDesk optics, as well as the loss incurred by the 50ft measurement fiber. The ScienceDesk optics does a 50% / 50% beam splitting in order to pipe the flux into both the laser powermeter and the CCD. This loss, plus the loss due to the transmission and reflection losses incurred by the mirrors and the focusing lens, gives a total transmission of $\sim$ 40%, which was confirmed by a direct laser powermeter measurement. For measurement at the fiber output we have an additional uncoated collimating lens right after the fiber holder, as well as the 50ft fiber. So we budget a total transmission loss due to the measurement optics on the CCD path of 35%. Dividing the photon flux measured at the CCD by 0.35, we obtain that the photon flux at the input of the APD is approximately 2.5×10^{12} photons per second (we ignored the coupling and transmission loss due to the last segment of the fiber leading to APD, since under the large reverse bias for the APD we are using part of this loss could be offset by the quantum efficiency increase over the nominal values on the APD. See the discussion in the next paragraph).

Now, taking into account that the product of the APD quantum efficiency and probability of detection is 0.3 at the HeNe frequency (from manufacturer's specifications. Note that this number is uncertain since we have currently applied a higher reverse bias to the APDs than the end point of the manufacturer's recommendations, so the actual product could be higher than 0.3. But on the other hand we did not directly measure the last segment of the fiber for both the coupling loss and the transmission loss, so in some ways these gain and loss effects are expected to partially cancel one another), we obtained that the APD afterpulsing rate is 1.6 and 4, respectively,

as measured with the two sets of ND filters, for channel 32 on spectrometer 3. The other channels measured for this spectrometer (i.e., channels 1, 10, and 20) gave afterpulsing rate in the similar range, but since they have only been measured with one set of filters we cannot have a good idea of the error bounds, and thus we will not report the result here. So it is most likely that we have a serious afterpulsing issue to deal with, even given the uncertainties of the current measurements.

3.8 Overall System Throughput Performance

Here is a summary of the relative throughput-loss contributions of the different segments of the NPOI optical train, for a "typical" beam path (in this case we choose it to be Astrometric Center station, on beam 2, passing through the science beam splitters A and B with one transmission followed by one reflection, to go into beam Spectrometer 3 (and we choose channel 20 to be a typical channel). All the numbers below are converted to single-pass equivalent throughput:

Feed system: 0.75
FDL path: 0.73
Spectrometer injection optics: 0.46
Beam splitters: 0.5.8=0.4 (here we accounted for the loss due to the output ports not used, but folded in the contribution from the other spectrometer where photons will be received and used)
Lenslet array/first fiber path: 0.78
Detector QE*PD: 0.3

We caution here once again that the detector quantum efficiency and probability of detector is uncertain due to the higher reverse bias we used.

The total throughput of the system, from multiplying the above numbers together, is 0.024, or 2.4%, close to the estimates obtained by various parties in the past at the HeNe frequency. We note again that this throughput number takes into account the loss due to the un-used ports of one set of beam splitting, but folded-in the photon contribution from the second set of beam splitting which distributes the photons evenly to two spectrometers. The abnormal beamline such as beam 6 will have correpondingly lower total throughput value.

The relative contributions of the frontend and the backend for a typical

NPOI beamline is:

Frontend (feed system and the FDL path including switchyard optics): 0.55
Backend (beam combiner table optics, unused ports, detector): 0.043

It is clear from the relative magnitude of these two numbers that the backend (optics, detectors, and un-used ports) contributed more than 10 times as much to the overall throughput loss as the frontend optics (mirrors, plus their propagation paths, and a couple windows).

Henrique Schmitt had previously derived the overall throughput numbers through stellar photometry, by comparing the embedded system count rates at the backend and the expected photon flux at the SID mirrors. These numbers can be found on WIKI site $http://sextans.lowell.edu/cgi-bin/wiki.cgi?ThroughputEstimates$. Henrique's numbers used the convention which did not fold in the contribution from the other spectrometer, and for the Astrometric Center Station on Spectrometer 3, near the HeNe frequency, he obtained an overall throughput of 1.99 %. In order to compared with the numbers we have obtained, we need to divide our numbers by 2 to account for the second beam splitting. Also, we need to divide Henrique's result by 0.633 to take into account of the sample-time correction which we have previously made to our count-rate measurement. So, it becomes 1.2% compared with Henrique's 3.14%, indicating a factor of ~ 2.6 in APD afterpulsing rate.

In actuality, since there is seeing-induced throughput loss, the likely transmission for observing a stellar source should be lower than using the laser source – thus indicates higher afterpulsing rate than the 2.6 given above. On the other hand, other factors such as the conversion of double-pass to single-pass throughput, and the detector quantum efficiency uncertainties, could partially offset this effect. So, until we perform the actual stellar throughput measurements, and find other means to estimate the detector quantum efficiency at the bias voltage we are using, we cannot be certain about the magnitude of afterpulsing from the stellar photometry side.

We note also that the direct stellar differential throughput measurements in comparison with the embedded system readout for the same stars give an afterpulsing rate that is independent of the CCD sensitivity calibration, and thus serves as a cross-comparison with the afterpusling rate estimate in the previous section. It is encouraging that these rates are in the similar range. The rates derived in the current work are also roughly consistent with the statisical models and autocorrelation studies of the APD counts of

D. Mozurkewich, though further analysis of the APD data taken earlier this year is needed for a more quantitative comparison.

3.9 Some Lessons Learned

Below are some insights gained during the first set of throughput tests, the implementation of which could enable a faster and bester future test procedure:

- One of the biggest time-sinkers during this first set of throughput test turned out to be the optical alignment, between the periscope (sometimes an additional collimating lens in front of it) on the beam combiner table, the periscope on the ScienceDesk, and the rest of the ScienceDesk optics. Part of the reasons that the alignment took longer than expected is that we ended up not being able to use the four degrees of freedom of adjustment offered by the two fold mirrors in the "figure 4" configuration on the ScienceDesk, due to the fact that these were both 2-inch mirrors, and when used in the current fold configuration vignetting is barely avoided for the 1.4 inch NPOI optical beam in the backend, and any significant adjustment on these two mirrors poses the danger of not being able to recover the position of vignetting avoidance. In the future, we will consider purchasing slightly larger mirrors to replace these two mirrors, so that we can make full and liberal use of the adjustment freedom provided by these mirrors, and speed up the alignment process each time we switch measurement position. With the near and far targets we currently use, both the lateral position and the angle of the optical beam on the ScienceDesk can be fixed between measurements.
- Upon analyzing the data, and comparing the laser powermeter and the CCD measurements, it is apparent that the highest data quality were obtained when the "before" and "after" measurements in the differential measurement were conducted both using the same CCD integration time, integration box, the same beam-combiner and ScienceDesk ND filter settings, and with CCD flux level set as close as possible to the middle of the dynamical range. This provides the least dependence on component calibration uncertainties and CCD nonlinearity. The data taken under these conditions (i.e., for the FDL paths and for the feed system) most often resulted in the agreement between the laser-powermeter-measured throughput and the CCD-measured throughput

within a few percent of each other. The long-term stability and repeatability of the measurement results under this kind of setup are also exceedingly good. On the other hand, the measurements we had to make where beams of different collimation properties and diameters were used, the agreement between the laser powermeter and the CCD results were poorer, though the main trend of variation were always given consistently by the laser and the CCD.

- During the tests we have encountered problems with not getting enough whitelight flux to do spectral throughput test, using the spectral filters on the ScienceDesk which have bandwidth on the order of 80 nm. We have thought of several possible remedies. The most expensive solution is to buy a tunable laser, or several single frequency lasers spread out over the visible bandpass. Another alternative is to purchase a Xenon or mercury arc lamp which have higher surface brightness (Xenon's bightness temperature is about twice as much as a QTH source, therefore is a factor of 16 larger in surface brightness). Yet other alternatives include modifying the existing whitelight injection optics, such as a bigger pinhole (the current one is likely to be 10μm, and we might be able to get away with a 50μm pinhole, but will need to verify the vignetting issue), or/and a different microscope objective for the pinhole to make the outgoing beam bundle more concentrated. It is desirable to get a factor of 20-30 increase in whitelight flux for a stable and reliable spectral throughput measurement. Finally, there is also the possibility to used an intensified CCD (or other high QE and low readnoise CCD). This last choice now appears most appealing since it also solves the problem of the spectral throughput measurement on stellar sources. The bright stellar sources have similar flux as the current whitelight source, and thus more sensitive CCD is needed both for the throughput measurements and also for the Risley prism tests.

3.10 Recommendations

Based on the preliminary analyses of the first set of throughput test results, we make the following recommendations for the follow-up tests, modeling, and for planning future upgrades of the system:

1. More permanent and stable mounts of the ND filters currently reside on the beam combiner table should be made, and the accurate calibration

of the attenuation values of the ND filters in their mounts need to be made.

2. New spectral light sources with high output flux, and/or image intensifiers, need to be implemented to enable the future spectral throughput measurements.

3. The dependence of FDL optical path throughput on pathlength, and on wavelength can already be explored by using the existing whitelight source on the beam combiner table and embedded system recording of channel flux at the different settings of the delay line. Hernrique Schmitt is now looking into this (he had found some tentative evidence of the delayline-length dependence of the throughput from the analysis of the stellar photometry data, but the seeing dependence of the throughput made the trend less apparent for most of the cases).

4. Future stellar measurements of the throughput using the same ScienceDesk optics and in the single-pass configuration will help to tie together the results of the double-pass measurements using artificial sources, and those inferred using the known magnitudes of stars and the flux recorded by the embedded system. If the throughput of the different segments of the optical path is indeed wavefront dependent (as it seems to be), it might be worthwhile to conduct stellar throughput measurements under the different seeing conditions. Such a test may be conducted even before the new whitelight source/image intensifier is implemented, whose result will help settle the APD afterpulsing issue (and this APD afterpulsing estimates would be totally independent of the CCD photometric calibration). This follow-up test can be joined together with the Risley prisms pilot test since they both employ stellar observations.

5. Direct wavefront measurements at the different locations along the optical path, as suggested by Sergio Restaino, will also provide valuable information on disentangling the contributions of large- and small-scale wavefront imperfections.

6. ZEMAX modeling effort should follow the successive throughput measurements to facilitate the understanding of the results obtained, and to reproduce through the incorporation of physical effects such as scattering, diffraction, transmission, etc. the actual performance of the system.

7. Though the upcoming whitelight and stellar throughput measurements still require the participation of the DC crew, it is recommmended that

the on-site personnels start to receive trainings in the measurement procedure so that they can take over further more detailed throughput characterizations of the system, the long-term monitoring of the system performance, as well as the characterization of the behavior of new optics being brought online, such as the long delayline (as suggested by Jim Clark).

8. Finally, one of the important realizations during the analyses of the throughput test results is that the NPOI system throughput loss is contributed much more by the backend (optics, detectors, and unused ports) than the frontend, with a factor of more than 10 difference in relative contributions between these two segments. This argues strongly for designing and builting a second-gneration NPOI backend beam combiner, utilizing the state-of-the-art optical fiber/integrated optics technologies and high quantum-efficiency detectors, so as both to improve (or at least to match) the throughput performance of the existing backend, but more importantly to allow better spatial filtering and photometric calibration capabilities, as well as the flexibility to separate fringer tracking and science observations. These, together with the bigger telescopes planned for the near future, will allow both the improved data quality and the observation of stars of fainter magnitudes.

Acknowledgments

During the year-long preparation process which led to the first set of throughput tests, a lot of people have contributed their talent, labor, and moral support to make the endeavor finally a success. Brit O'Neill and Dave Mozurkewich participated in the data acquisition process of the test week, whose familiarity with the operations of the existing instrument and experiene with the alignment and trouble-shooting processes were vital to the success of the test efforts. In addition, Brit contributed to a number of preparations steps for the test, and also took care of the most risky part of the experiment: the placement and removal of the periscope on the beam combiner table, which she did without a hitch. Throughout the different stages of the throughput test preparation Dave's continued interests and input were both inspirational and extremely helpful; much appreciated was also his diligence in accomplishing every support task during the test week, and the care he took in monitoring the data quality through the Obslog while

Brit and I worked in the inner room.

Jim Clark and Josh Walton were responsible for modifying the Newport periscope used on the beam combiner table with features which made it stable and safe. JC and Josh also took care of receiving the steady streams of hardware we shipped to the site, and participated in the assembly and transport of the ScienceDesk which housed most of the throughput test optics.

The management at NRL, e.g. the PI Tom Armstrong and Branchhead Charmaine Gilbreath, provided the much needed institutional support and financial backing. The fellow scientists and engineers at NRL supported the endeavor with both their enthusiasm and their inputs. Memebers of the Design Review Committee, Don Hutter, Nat White and Jim Clark provided valuable input during the preliminary and critical design review phases of the project. The technical advisor Jim Benson contributed thoughtful ideas which improved the implementation of the test configuration.

I thank all of you on the NPOI team whose support and help were vital to the successful carrying out of this project.

Appendix. CCD Sensitivity and Gain Factor

The CCD camera we used in the throughput test is of Adimec 1000M, with an internal Kodak CCD chip. The manufacturer-quoted sensitivity is 5.5 lux for 100% video, 33 millisecond integration, for a 3200 K light source with BG 38-1 mm color glass filter.

If the camera is used in the 10-bit mode, the above sensitivity translates to

$$Sensitivity(\lambda_{cal})_{10-bit} = \frac{1024}{5.5} \times 33 = 6144\ counts/lux/sec \qquad (1)$$

for a single pixel. This compares well with the sensitivity of another Kodak/Roper camera I had used before, i.e. model ES-310, which has a sensitivity of 6400 10-bit counts/lux/sec.

However, we have used the camera in the 8-bit mode in the August tests, since the software needed for supporting the 10-bit mode was not yet implemented. I have recently confirmed through lab tests that in the 8-bit mode the apparent sensitivity (in terms of counts per lux per second) is 4 times less than the 10-bit mode, even though in actuality the same number of lux

per second fills the full-well in both cases (i.e., the full-well is represented by the different number of bits in each case). Therefore, the sensitivity for the 8-bit mode is

$$Sensitivity(\lambda_{cal})_{8-bit} = \frac{256}{5.5} \times 33 = 1536 \; counts/lux/sec. \tag{2}$$

In the following calculations we will use only the 8-bit sensitivities.

The above sensitivity is measured presumably at a wavelength, which we call λ_{cal}, which falls in the blue-green region (thus the name of the color filter BG-38) of the visible spectrum, i.e., with wavelength range of 450-500 nm. For other wavelengths, the Adimec specification gives rather the quantum efficiency of the CCD. In general,

$$Sensitivity(\lambda) = Sensitivity(\lambda_{cal}) \times \frac{QE(\lambda)}{QE(\lambda_{cal})} \tag{3}$$

where λ_{cal} in this case happens to be near the peak of the CCD quantum efficiency curve ($QE_{cal} \approx 0.45$)). So at the HeNe frequency used in our first set of tests, since QE(633nm)=0.27, therefore the sensitivity of the CCD at the HeNe frequency is

$$\begin{aligned} Sensitivity(633nm) &= 1536 \; counts/lux/sec \cdot 0.27/0.45 \\ &= 921.5 \; counts/lux/sec \end{aligned} \tag{4}$$

Now 1 lux = 1 lumen/m^{-2}. Also, the definition of lumen is such that 1 watt of optical flux at 555 nm gives the same physical sensation as 680 lumen. Define $K_m = 680 \; lm/W$, we have that at other wavelengths

$$K_\lambda = K_m y_\lambda = 680 \; y_\lambda lm/W \tag{5}$$

where the normalized conversion factor y_λ is a bell-shaped curve with wavelengths, peaked at 555 nm with value 1, and drops to zero at the two ends around 400 and 700 nm, respectively. Fortunatly, the original sensitivity number was given at a wavelength close to the peak of the conversion curve, so we will just use conversion factor 680 to convert the sensitivity to the SI units.

With these information we can now calculate the conversion factor between the effective incident photon rate and the integrated count rate measured by the CCD (which has a linear pixel size of 7.4 μm):

$$\#ofphotons/sec = \frac{Energy/sec}{h\nu} \tag{6}$$

$$= \frac{(\#\ of\ integrated\ counts/sec) \cdot (pixel\ area\ in\ m^2)}{(Sensitivity\ in\ counts/lux/sec/pixel) \cdot 680\ lm/W \cdot h\nu}$$

$$= \frac{(\#\ of\ integrated\ counts/sec) \cdot (7.5 \cdot 10^{-6})^2}{921.5 \cdot 680 \cdot 6.62 \cdot 10^{-34} \cdot 3 \cdot 10^8 / 633 \cdot 10^{-9}}$$

$$= 286 \times (\#\ of\ integrated\ counts/sec),$$

the above conversion factor of course is specifically for photons at HeNe frequency. At a different wavelength a new gain factor will have to be calculated.